Self-diffusiophoresis with bulk reaction

Rodolfo Brandão ⓘ

*Department of Mechanical and Aerospace Engineering, Princeton University, Princeton,
New Jersey 08544, USA*

Gunnar G. Peng ⓘ

Department of Mathematics, Imperial College London, London SW7 2AZ, United Kingdom

David Saintillan ⓘ

*Department of Mechanical and Aerospace Engineering, University of California San Diego,
La Jolla, California 92093, USA*

Ehud Yariv ⓘ

*Department of Mechanical and Aerospace Engineering, Princeton University,
Princeton, New Jersey 08544, USA
and Department of Mathematics, Technion — Israel Institute of Technology, Haifa 32000, Israel*

We consider phoretic self-propulsion of a chemically active colloid where solute is produced on the colloid surface (with a spatially varying rate) and consumed in the bulk solution (or vice versa). Assuming first-order kinetics, the dimensionless transport problem is governed by the surface Damköhler number $\mathcal{S}$ and the bulk Damköhler number $\mathcal{B}$. The dimensionless colloid velocity U, normalized by a self-phoretic scale, is a nonlinear function of these two parameters. In the limit of small $\mathcal{S}$, the solute flux is effectively prescribed by the surface activity distribution, resulting in an explicit expression for U that is proportional to $\mathcal{S}$. In the limit of large $\mathcal{B}$, the deviations of solute concentration from the equilibrium value are restricted to a narrow layer about the active portion of the colloid boundary. The associated boundary-layer analysis yields another explicit expression for U. Both asymptotic predictions are corroborated by an eigenfunction expansion solution of the exact problem for the cases when all physical parameters are held fixed except for a varying colloid size (resulting in $\mathcal{S} \propto \mathcal{B}^{1/2}$) or a varying solute diffusivity (resulting in $\mathcal{S} \propto \mathcal{B}$). The boundary-layer structure breaks down near the transition between the active and inactive portions of the boundary. The local solution in the transition region partially resembles the classical Sommerfeld solution of wave diffraction from an edge.

I. INTRODUCTION

The remarkable propulsion exhibited by chemically active particles in liquid solutions, known as self-diffusiophoresis, has garnered significant attention following experimental breakthroughs in catalytic swimmers [1]. The fundamental mechanism underpinning phoretic self-propulsion involves two key components: solute production or consumption at the particle boundary, coupled with short-range interactions between the solute molecules and that boundary. Golestanian *et al.* [2] introduced the first macroscale model to describe self-diffusiophoresis under Stokes flow conditions, accounting for diffusive solute transport. In that model, chemical reactions at the particle boundary are represented through a prescribed solute flux distribution, while mechanical interactions with

solute molecules are captured through a diffusio-osmotic slip velocity—proportional to the tangential solute gradient at the outer edge of the interaction layer [3]. In the absence of solute advection, the linearity of the governing equations and boundary conditions implies that an asymmetry in the particle shape or physicochemical properties is required for self-propulsion: in typical experiments involving spherical colloids, this asymmetry is achieved by coating half of a particle with a catalyst.

A more sophisticated model of surface reactions involves first-order chemical kinetics [4]. The associated boundary condition imposes a linear relation between the solute flux and the local excess concentration, whose characteristic ratio defines the surface Damköhler number (hereafter denoted by $\mathcal{S}$). For slow reaction rates ($\mathcal{S} \to 0$), the imposed flux model is recovered. Accounting for finite Damköhler number has proven to be essential for capturing the dependence of the propulsion speed on particle size, as observed in experiments [4].

Of interest to us in this work is the case where the excess solute gets consumed or produced in the bulk liquid surrounding the particle, for instance as a result of chemical degradation or bulk reaction with another solute. In that case, the strength of consumption is characterized by a bulk Damköhler number, hereafter denoted by $\mathcal{B}$, defined as the ratio of the reactive to diffusive consumption rates. Solute bulk consumption has already been studied using both numerical simulations [5] as well as weakly nonlinear analyses near the threshold for spontaneous motion [6]. In certain singular problems (e.g., involving two-dimensional [7–9] or channel [10,11] geometries), even a weak bulk reaction may have significant effect.

Here, we analyze the steady self-diffusiophoresis of a spherical particle. The paper is organized as follows. In Sec. II we present the physicochemical problem, constructing the kinetic model with some care (which is often absent in the prevailing literature on self-diffusiophoresis). The dimensionless problem is formulated in Sec. III, where we define the two Damköhler numbers. An exact solution based upon an eigenfunction expansion is derived in Sec. IV. Asymptotic approximations for both small $\mathcal{S}$ and large $\mathcal{B}$ are discussed in Sec. V. The boundary-layer analysis in the latter limit may break down near the junction between the active and inert portions of the particle boundary. We analyze the structure of this transition region in Sec. VI. Illustrative examples are presented in Sec. VII. We conclude in Sec. VIII.

II. PHYSICAL PROBLEM

A chemically active spherical particle of radius a^* is freely suspended in an unbounded liquid solution. (Hereafter, dimensional quantities are decorated by an asterisk.) The driver for self-diffusiophoresis is an inhomogeneous chemical reaction at the particle boundary. For simplicity, we assume that the surface patterning (e.g., a catalyst) is symmetric about an axis passing through the particle center. Our interest is in the steady-state transport occurring in a particle-fixed reference system; to that end, we employ the spherical polar coordinates (a^*r, θ, ϖ), with $r = 0$ at the particle center and $\theta = 0, \pi$ being the symmetry axis, see Fig. 1. Given the presumed axial symmetry, the solute concentration c^* is a function of r and θ. Our goal is the velocity of that system relative to the otherwise quiescent liquid. That velocity must be parallel to the symmetry axis, say $U^*\hat{\imath}$ ($\hat{\imath}$ being a unit vector in the direction $\theta = 0$).

Suppose first that a reversible surface reaction generates solute from one or more abundant species whose concentrations c_i^* may be regarded as constant. We assume that the surface patterning affects both the forward and backward reaction rates in the same spatial manner, say in proportion to a (dimensionless) non-negative distribution $f(\theta)$. The forward and backward rates are, respectively,

$$k_+^* f(\theta) \prod_i c_i^*, \quad k_-^* f(\theta) c^*, \tag{2.1}$$

wherein $k_\pm^*$ are the forward and backward rate constants. (In particular, $k_\pm^*$ has the dimensions of velocity.) The production/absorption condition at the particle boundary is accordingly

$$-\frac{D^*}{a^*} \frac{\partial c^*}{\partial r} = k_-^* (c_s^* - c^*) f(\theta) \quad \text{at} \quad r = 1, \tag{2.2}$$
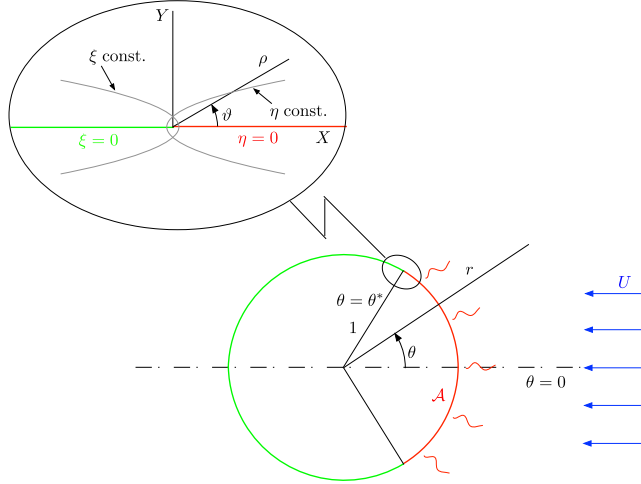
FIG. 1. Schematic showing the particle geometry and coordinates. The zoomed region (rotated) describes the transition-region coordinates.

wherein D^* is the solute diffusivity and

$$c_s^* = (k_+^*/k_-^*) \prod_i c_i^* \tag{2.3}$$

is the equilibrium concentration for the surface reaction. The model (2.2) also describes the simpler irreversible case where the surface patterning catalyzes a breakdown of the solute with no replenishment, for which $c_s^* = 0$.

We model the production or consumption of solute in the bulk in the same way as on the surface, but without any spatial variation. In other words, the solute is consumed at a volumetric rate provided by the product of c^* with a uniform bulk rate constant, say k_b^* (with the dimensions of inverse time), and may be replenished by a reaction (which need not be the reverse of the consumption reaction) at a uniform rate which can then be written as $k_b^* c_b^*$. The constant c_b^* may therefore be interpreted as an equilibrium concentration—the bulk analog of c_s^*. Overall, then, solute is consumed in the bulk in proportion to the excess concentration $c^* - c_b^*$ with a uniform bulk rate constant k_b^* [5,12]:

$$\text{bulk consumption (per unit volume)} = k_b^*(c^* - c_b^*). \tag{2.4}$$

For true chemical degradation, where $c_b^* = 0$, Eq. (2.4) represents a pure decay of the solute by a first-order chemical reaction with no replenishment.

At steady state, it follows that c^* satisfies the diffusion-reaction equation

$$\frac{D^*}{a^{*2}} \nabla^2 c^* = k_b^*(c^* - c_b^*) \quad \text{for} \quad r^* > a^*, \tag{2.5}$$

in which solute advection has been neglected. Due to axial symmetry, the dimensionless Laplacian adopts the form

$$\nabla^2 = \frac{1}{r^2} \frac{\partial}{\partial r} \left(r^2 \frac{\partial}{\partial r} \right) + \frac{1}{r^2 \sin\theta} \frac{\partial}{\partial \theta} \left(\sin\theta \frac{\partial}{\partial \theta} \right). \tag{2.6}$$

The concentration c^* is governed by Eq. (2.5), together with condition (2.2) and the requirement of far-field approach to c_b^*. The concentration c^* consequently lies between c_s^* and c_b^*. Hence either $c_b^* < c^* < c_s^*$, leading to production on surface and consumption in the bulk, or $c_s^* < c^* < c_b^*$, leading to production in the bulk and consumption on the surface.

In describing the hydrodynamic problem we employ a macroscale description, where the short-range interaction between the solute molecules and the particle is manifested by diffusio-osmotic slip [3],

$$\text{slip velocity} = -b^* \times \text{surface gradient of solute concentration.} \tag{2.7}$$

We assume that b^* is uniform. Note that b^* is a signed quantity, positive for attractive interactions and negative for repulsive ones [3]. The fluid velocity in the comoving frame is therefore governed by the continuity and Stokes equations together with condition (2.7) and the requirement for approaching the uniform velocity $-U^*\hat{\imath}$ at large distances. Consistently with the macroscale description, the particle acquires the rectilinear velocity U^* required to keep it force-free.

III. DIMENSIONLESS FORMULATION

Relation (2.2) leads to the definition of the surface Damköhler number

$$\mathcal{S} = \frac{k_-^* a^*}{D^*}, \tag{3.1}$$

representing the ratio of reactive to diffusive solute flux densities. Equation (2.5) leads to the definition of the bulk Damköhler number

$$\mathcal{B} = \frac{k_b^* a^{*2}}{D^*}, \tag{3.2}$$

representing the ratio of reactive to diffusive consumption rates. As will become evident from the equations below, the dimensionless problem depends only upon these two parameters.

We define the dimensionless concentration c by

$$c^* = c_b^* + (c_s^* - c_b^*)c. \tag{3.3}$$

This nondimensionalization renders $0 < c < 1$. For $c_b^* < c_s^*$, the quantity c represents the excess concentration relative to the bulk. For $c_s^* < c_b^*$ it measures the concentration deficit relative to the bulk. The dimensionless fluid velocity is obtained by normalizing the dimensional velocity with

$$\mathcal{U}^* = \frac{b^*(c_s^* - c_b^*)}{a^*}. \tag{3.4}$$

The dimensionless solute transport problem is governed by: (i) the modified Helmholtz equation [cf. Eq. (2.5)]

$$\nabla^2 c = \mathcal{B}c; \tag{3.5}$$

(ii) the kinetic condition at the particle boundary [cf. Eq. (2.2)]

$$\frac{\partial c}{\partial r} = -\mathcal{S}(1 - c)f(\theta) \quad \text{at} \quad r = 1; \tag{3.6}$$

and (iii) the approach to equilibrium at large distances

$$c \to 0 \quad \text{as} \quad r \to \infty. \tag{3.7}$$

Since solutions to the modified Helmholtz equation decay exponentially fast [cf. Eq. (4.2)], there is no solute flux from infinity. From a conservation point of view, then, the surface and bulk processes must be opposite at steady state.

The problem specified by Eqs. (3.5)–(3.7) defines c as a function of the governing parameters $\mathcal{S}$ and $\mathcal{B}$, as well as the activity distribution $f(\theta)$. Once solved, we can consider the flow, governed by: (i) the continuity and Stokes equations; (ii) the diffusio-osmotic slip [cf. Eq. (2.7)]

$$\mathbf{u} = -\hat{\mathbf{e}}_\theta \frac{\partial c}{\partial \theta} \quad \text{at} \quad r = 1; \tag{3.8}$$

(iii) the far-field approach to a uniform stream (see Fig. 1)

$$\mathbf{u} \to -U\hat{\imath} \quad \text{as} \quad r \to \infty, \tag{3.9}$$

where $U = U^*/\mathcal{U}^*$; and (iv) the requirement that the particle is force-free. In fact, the detailed calculation of the flow field is not required, as use of the reciprocal theorem [13] provides U as the quadrature

$$U = -\frac{1}{2} \int_0^\pi \left. \frac{\partial c}{\partial \theta} \right|_{r=1} \sin^2 \theta \, d\theta, \tag{3.10}$$

or, following integration by parts,

$$U = \int_0^\pi c|_{r=1} \sin \theta \cos \theta \, d\theta. \tag{3.11}$$

In what follows, it may be convenient to employ $\mu = \cos \theta$ instead of θ. Writing $f(\theta) = F(\mu)$, it is natural to represent F as a series of surface harmonics,

$$F(\mu) = \sum_{m=0}^\infty F_m P_m(\mu), \tag{3.12}$$

wherein P_m are the Legendre polynomials of degree m. Using the orthogonality of these polynomials,

$$\int_{-1}^1 P_m(\mu)P_n(\mu) \, d\mu = \frac{2}{2m+1}\delta_{mn}, \tag{3.13}$$

we obtain

$$F_m = \frac{2m+1}{2} \int_{-1}^1 F(\mu)P_m(\mu) \, d\mu. \tag{3.14}$$

When using μ, Eq. (3.11) simplifies to

$$U = \int_{-1}^1 \mu \, c|_{r=1} \, d\mu, \tag{3.15}$$

where, with a slight abuse of notation, c is regarded as a function of r and μ.

IV. EXACT SOLUTION

Using the eigenfunctions of the modified Helmholtz equation, we find that the most general axisymmetric solution of Eqs. (3.5)–(3.7) is

$$c = \sum_{n=0}^\infty A_n \phi_n(r) P_n(\cos \theta), \tag{4.1}$$

where

$$\phi_n(r) = r^{-1/2} K_{n+1/2}(\mathcal{B}^{1/2} r), \tag{4.2}$$

in which K_ν is the modified Bessel function of the second kind with degree ν. Substitution of Eqs. (3.12) and (4.1) into condition (3.6) yields

$$\sum_{n=0}^\infty A_n \phi_n'(1) P_n(\mu) = -\mathcal{S}\left[1 - \sum_{n=0}^\infty A_n \phi_n(1) P_n(\mu) \right] \sum_{m=0}^\infty F_m P_m(\mu), \tag{4.3}$$

where the prime denotes differentiation with respect to the argument. Projection of Eq. (4.3) upon $P_n(\mu)$ ($n = 0, 1, 2, \ldots$) yields an infinite linear system governing the coefficients $\{A_n\}_{n=0}^\infty$. Using

controlled truncation, this system may be solved in principle for any values of $\mathcal{B}$ and $\mathcal{S}$ and a given activity distribution $f(\theta)$. Once solved, substitution into Eq. (3.15) yields, upon making use of the orthogonality relations (3.13)

$$U = \tfrac{2}{3} A_1 \phi_1(1). \tag{4.4}$$

Prior to illustrating the exact solution for a specific activity distribution, it is desirable to supplement it by asymptotic approximations.

V. ASYMPTOTIC APPROXIMATIONS

A. Linked Damköhler numbers

Considering the manner by which the Damköhler numbers (3.1)–(3.2) depend upon the dimensional quantities in the problem, there are two natural scenarios where these two numbers are linked. When the particle size a^* is allowed to vary while all other dimensional quantities are fixed, the linkage

$$\mathcal{S} = \alpha \mathcal{B}^{1/2} \tag{5.1}$$

emerges, where $\alpha = k_-^*/(D^* k_b^*)^{1/2}$ is fixed. When instead the diffusivity D^* is varied, the linkage

$$\mathcal{S} = \beta \mathcal{B} \tag{5.2}$$

is obtained, where $\beta = k_-^*/(a^* k_b^*)$ is fixed.

We will next consider asymptotic limits where $\mathcal{S}$ is small or $\mathcal{B}$ is large. The linkages above suggest that, in these limits, $\mathcal{B}$ is small and $\mathcal{S}$ is large, respectively. However, depending on the values of α or β, in practice $\mathcal{S}$ could have a small numerical value at the same time as $\mathcal{B}$ has a large one. Hence, in the analysis for small $\mathcal{S}$ we do not make any assumption from the outset on the size of $\mathcal{B}$, and vice versa.

B. Small surface Damköhler number

For small Damköhler surface number $\mathcal{S} \ll 1$, it is evident from Eq. (3.6) that c is of order $\mathcal{S}$. It then follows that the surface solute flux becomes directly prescribed by $f(\theta)$, independent of the concentration. We therefore find from Eq. (4.3)

$$A_n \approx -\frac{\mathcal{S} \phi_n(1)}{\phi_n'(1)} F_n. \tag{5.3}$$

The particle velocity is then obtained from Eq. (4.4):

$$U \approx -\frac{2\mathcal{S}\phi_1(1)}{3\phi_1'(1)} F_1, \tag{5.4}$$

or, upon using Eq. (4.2),

$$U \approx \frac{2\mathcal{S}(1 + \mathcal{B}^{1/2})}{3(2 + 2\mathcal{B}^{1/2} + \mathcal{B})} F_1. \tag{5.5}$$

We note that the asymptotic error in Eq. (5.5) is $O(\mathcal{S}^2)$. It follows that for $\mathcal{B} = O(\mathcal{S})$—which includes both linkages (5.1) and (5.2)—approximation (5.5) is asymptotically equivalent to

$$U \approx \frac{\mathcal{S} F_1}{3}, \tag{5.6}$$

with an $O(\mathcal{S}^2)$ asymptotic error. We have therefore retrieved the well-known result [2] in the absence of bulk reaction. For large $\mathcal{B}$, on the other hand,

$$U \approx \frac{2\mathcal{S}F_1}{3\mathcal{B}^{1/2}}. \tag{5.7}$$

C. Large bulk Damköhler number

In the limit of large bulk Damköhler number, $\mathcal{B} \gg 1$, we find from Eqs. (3.5) and (3.7) that

$$c \equiv 0. \tag{5.8}$$

Since this is an exact solution of both Eqs. (3.5) and (3.7), it is evident the asymptotic error is exponentially small.

The trivial solution (5.8) is clearly incompatible with condition (3.6). Seeking an additional distinguished limit at large $\mathcal{B}$, we observe from Eq. (3.5) a dominant balance with spatial variations across a narrow region of ord($\mathcal{B}^{-1/2}$) width. We therefore postulate a boundary layer of that width about the particle boundary $r = 1$. Defining the stretched coordinate

$$Y = \mathcal{B}^{1/2}(r - 1), \tag{5.9}$$

we write in the boundary layer

$$c(r, \theta; \mathcal{B}) = \tilde{c}(Y, \theta; \mathcal{B}). \tag{5.10}$$

Substitution of Eqs. (5.9)–(5.10) into the diffusion-reaction equation (3.5) yields

$$\frac{\partial^2 \tilde{c}}{\partial Y^2} \approx \tilde{c} \quad \text{for} \quad Y > 0. \tag{5.11}$$

Condition (3.6) becomes

$$\mathcal{B}^{1/2} \frac{\partial \tilde{c}}{\partial Y} = -\mathcal{S}(1 - \tilde{c})f(\theta) \quad \text{at} \quad Y = 0, \tag{5.12}$$

and the requirement of matching with the "outer" solution (5.8) implies the far-field decay

$$\lim_{Y \to \infty} \tilde{c} = 0. \tag{5.13}$$

The solution of Eqs. (5.11)–(5.13) is simply

$$\tilde{c}(Y, \theta) \approx \frac{\mathcal{S}f(\theta)}{\mathcal{S}f(\theta) + \mathcal{B}^{1/2}} e^{-Y}. \tag{5.14}$$

Substitution into Eq. (3.11) then provides the particle velocity

$$U \approx \int_0^\pi \frac{\mathcal{S}f(\theta)}{\mathcal{S}f(\theta) + \mathcal{B}^{1/2}} \sin\theta \cos\theta \, d\theta. \tag{5.15}$$

Up to this point, the analysis has been carried out with no restrictions on $\mathcal{S}$. We note using Eq. (3.14) that for $\mathcal{S} \ll 1$ quadrature (5.15) readily reproduces Eq. (5.7). More generally, it is evident from Eq. (5.15) that the linkage (5.1) constitutes a distinguished limit at large $\mathcal{B}$, whereby

$$U \approx \int_{\mathcal{A}} \frac{\alpha f(\theta)}{1 + \alpha f(\theta)} \sin\theta \cos\theta \, d\theta. \tag{5.16}$$

For the case

$$\mathcal{S} \gg \mathcal{B}^{1/2}, \tag{5.17}$$

which includes (but is not restricted to) linkage (5.2), the fraction in the integrand of Eq. (5.15) somewhat surprisingly reduces to a discontinuous function: 1 where $f > 0$ and 0 where $f = 0$. We

therefore obtain

$$U \approx \int_{\mathcal{A}} \sin \theta \cos \theta \, d\theta, \tag{5.18}$$

wherein

$$\mathcal{A} = \{\theta \in (0, \pi) | f(\theta) > 0\} \tag{5.19}$$

is the active portion of the boundary (see Fig. 1). Remarkably, the particle velocity depends only upon the extent of the active portion of the boundary; in particular, it is insensitive to the details of the activity profile. In what follows, it is convenient to restrict the analysis to the case (see Fig. 1) where $\mathcal{A} = (0, \theta^*)$ with $0 < \theta^* < \pi$ [cf. Eqs. (7.1) and (7.4)]. Under this modest restriction, Eq. (5.18) gives

$$U = \frac{\sin^2 \theta^*}{2}. \tag{5.20}$$

VI. TRANSITION REGION

The asymptotic solution in the limit $\mathcal{B} \gg 1$ with $\mathcal{S} \gg \mathcal{B}^{1/2}$ may appear to introduce a contradiction. Indeed, the nonzero velocity (5.20), which may be traced back to Eq. (3.11), seems incompatible with the zero velocity predicted by a naive substitution into the original quadrature (3.10) of the limiting concentration [cf. Eq. (5.14)]:

$$\tilde{c}(Y, \theta) = \begin{cases} e^{-Y} & \text{for} \quad 0 < \theta < \theta^*, \\ 0 & \text{for} \quad \theta^* < \theta < \pi. \end{cases} \tag{6.1}$$

The origin of this incompatibility has to do with the edge $\theta = \theta^*$ of $\mathcal{A}$. With a finite discontinuity of $\tilde{c}$ there, expression (3.10) cannot be applied in a piecewise manner. The resolution of this apparent contradiction has to do with a breakdown of the boundary-layer structure. The boundary-layer solution, where variations with respect to θ are assumed "slow," is clearly incompatible with a finite discontinuity.

We therefore consider a transition region about the edge ($r = 1$ and $\theta = \theta^*$) of $\mathcal{A}$. In that region, the excess concentration smoothly varies between the two branches of Eq. (6.1). With the presence of such a region, the original quadrature (3.10) is dominated by a small neighborhood $\mathcal{N}$ of θ^*, which is still asymptotically larger than the width of the transition region. Since θ is approximately constant in that neighborhood, we obtain from Eq. (3.10)

$$U = -\frac{\sin^2 \theta^*}{2} \int_{\mathcal{N}} \frac{\partial c}{\partial \theta} \bigg|_{r=1} d\theta. \tag{6.2}$$

Recalling the need to match the unity value for $\theta < \theta^*$ and the zero value for $\theta > \theta^*$, we retrieve Eq. (5.20).

The boundary-layer scaling suggests that the lateral extent of the transition region is $\mathcal{B}^{-1/2}$. Defining the local coordinate [cf. Eq. (5.9)]

$$X = \mathcal{B}^{1/2}(\theta^* - \theta), \tag{6.3}$$

and considering the limit $\mathcal{B} \to \infty$ with X, Y fixed, we find that the transition region coincides with the upper half XY plane (see Fig. 1). Defining $C(X, Y) = c(r, \theta)$, C is governed by the modified Helmholtz equation

$$\frac{\partial^2 C}{\partial X^2} + \frac{\partial^2 C}{\partial Y^2} = C \quad \text{for} \quad Y > 0. \tag{6.4}$$

At large Y it must satisfy

$$\lim_{Y \to \infty} C = 0, \tag{6.5}$$

representing asymptotic matching with Eq. (5.8).

It remains to specify the mixed boundary conditions at $Y = 0$. Using definition (6.3), the exact condition (5.12) reads

$$\frac{\partial C}{\partial Y} = -\mathcal{S}\mathcal{B}^{-1/2}(1 - C)f(\theta^* - \mathcal{B}^{-1/2}X) \quad \text{at} \quad Y = 0. \tag{6.6}$$

In the inert portion of the boundary, where $f = 0$, we find

$$\frac{\partial C}{\partial Y} = 0 \quad \text{for} \quad X < 0. \tag{6.7}$$

The condition on the active portion depends upon the asymptotic behavior of $f(\theta)$ as $\theta \nearrow \theta^*$. To that end we consider two representative cases.

In the case where $f(\theta)$ attains a nonzero limit [cf. Eq. (7.1)] as $\theta \nearrow \theta^*$ we simply find from Eq. (5.17)

$$C = 1 \quad \text{for} \quad X > 0. \tag{6.8}$$

The resulting problem is reminiscent of the diffraction of plane waves of sound by the edge of a semi-infinite screen—a problem originally solved by Sommerfeld [14]. Defining the local polar coordinates (ρ, ϑ) by

$$X = \rho \cos \vartheta, \quad Y = \rho \sin \vartheta \tag{6.9}$$

(see Fig. 1), the solution of Eqs. (6.4)–(6.5) and Eqs. (6.7)–(6.8), derived in the Appendix, is

$$C = \frac{e^{-Y}}{2}\left\{1 + \text{erf}\left[\rho^{1/2}\left(\cos\frac{\vartheta}{2} - \sin\frac{\vartheta}{2}\right)\right]\right\} + \frac{e^{Y}}{2}\left\{1 - \text{erf}\left[\rho^{1/2}\left(\cos\frac{\vartheta}{2} + \sin\frac{\vartheta}{2}\right)\right]\right\}. \tag{6.10}$$

In terms of the polar coordinates (6.9), the limit $X \to \infty$ with Y fixed corresponds to $\rho \to \infty$ with $\vartheta = O(1/\rho)$. We then readily obtain

$$\lim_{X \to \infty} C = e^{-Y}, \tag{6.11}$$

which trivially matches the top branch of the boundary-layer solution (6.1). The limit $X \to -\infty$ with Y fixed corresponds to $\rho \to \infty$ with $\pi - \vartheta = O(1/\rho)$. Here, we obtain

$$\lim_{X \to -\infty} C = 0, \tag{6.12}$$

which trivially matches the lower branch of the boundary-layer solution (6.1).

In the case where $f(\theta) \sim K(\theta^* - \theta)$ as $\theta \nearrow \theta^*$ [cf. Eq. (7.4), where $K = 1$], condition (6.6) becomes

$$\frac{\partial C}{\partial Y} = -K\mathcal{S}\mathcal{B}^{-1}(1 - C)X \quad \text{for} \quad X > 0. \tag{6.13}$$

Here, it is evident that Eq. (5.2) is a distinguished limit, giving the condition

$$\frac{\partial C}{\partial Y} = -\beta K(1 - C)X \quad \text{for} \quad X > 0. \tag{6.14}$$

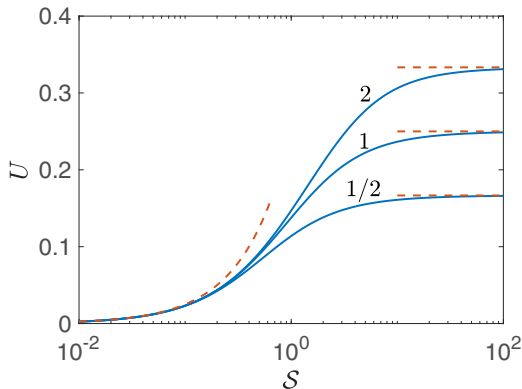We did not attempt to address the resulting mixed boundary-value problem.

FIG. 2. U versus $\mathcal{S}$ using linkage-by-size (5.1) for the Janus profile (7.1). Solid: exact result (4.4) for the indicated values of α. Dashed: small-$\mathcal{S}$ approximation (5.6) and large-$\mathcal{B}$ approximation (7.3).

VII. ILLUSTRATIONS

We continue by illustrating our results, considering first the case of linkage by size. With $\mathcal{B}$ locked to $\mathcal{S}$ via Eq. (5.1), U becomes a function of $\mathcal{S}$, α and the activity profile. We use a Janus configuration, namely,

$$f(\theta) = \begin{cases} 1, & 0 < \theta < \pi/2, \\ 0, & \pi/2 < \theta < \pi, \end{cases} \tag{7.1}$$

for which Eq. (3.14) gives

$$F_{2k} = \frac{\delta_{k,0}}{2}, \quad F_{2k+1} = \frac{(-)^k (2k)!(4k+3)}{2^{2k+2}(k!)^2(k+1)}, \tag{7.2}$$

and, in particular, $F_1 = 3/4$. The velocity calculated using Eq. (4.4) is shown in Fig. 2 for $\alpha = 1/2$, 1, and 2. We also portray the α-independent small Damköhler-number approximation (5.6), which here gives $U \approx \mathcal{S}/4$ for $\mathcal{S} \ll 1$. With Eq. (7.1), the large Damköhler-number approximation (5.16) gives

$$\lim_{\mathcal{S} \to \infty} U = \frac{\alpha}{2(1+\alpha)}. \tag{7.3}$$

For the aforementioned α values, Eq. (7.3) implies the respective limits 1/6, 1/4, and 1/3. The approach at large $\mathcal{S}$ to these limits is evident in the figure.

Consider now linkage by diffusivity. With $\mathcal{B}$ locked to $\mathcal{S}$ via Eq. (5.2), U becomes a function of $\mathcal{S}$, β and the activity profile. We here use a single linkage value, $\beta = 1$, but consider both the Janus activity distribution (7.1) and the generalized Janus profile

$$f(\theta) = \begin{cases} \cos\theta, & 0 < \theta < \pi/2, \\ 0, & \pi/2 < \theta < \pi, \end{cases} \tag{7.4}$$

for which

$$F_{2k} = \frac{(-)^{k+1}(2k)!(4k+1)}{4^{k+1}(k!)^2(k+1)(2k-1)}, \quad F_{2k+1} = \frac{\delta_{k0}}{2}, \tag{7.5}$$

and, in particular, $F_1 = 1/2$. For that profile the small Damköhler-number approximation (5.6) gives $U \approx \mathcal{S}/6$. Since $\mathcal{A} = (0, \pi/2)$ for both Eqs. (7.1) and (7.4), these distributions share the same large

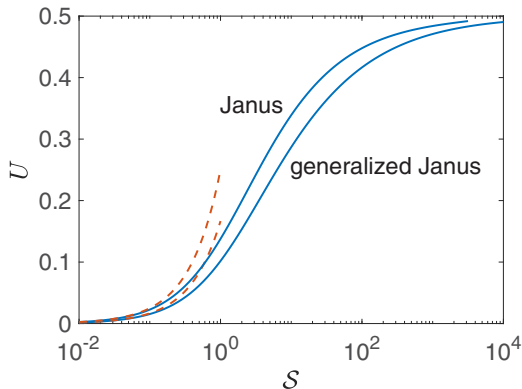FIG. 3. U versus $\mathcal{S}$ using linkage-by-diffusivity (5.2) with $\beta = 1$ for both the Janus (7.1) and the generalized Janus (7.4) activity profiles. Solid: exact result (4.4). Dashed: small Damköhler-number approximation (5.6).

Damköhler-number limit (5.20), namely,

$$\lim_{\mathcal{S} \to \infty} U = \tfrac{1}{2}. \tag{7.6}$$

The results are illustrated in Fig. 3.

In calculating U using Eq. (4.4), we have encountered difficulties when applying the numerical scheme at large values of $\mathcal{S}$. These are more pronounced for the Janus profile (7.1), where the interfacial activity undergoes a finite discontinuity at $\theta = \pi/2$. Apparently, the associated nonsmoothness escalates the Gibbs phenomenon. In any event, the approach to the limit (7.6) is unequivocal.

VIII. CONCLUDING REMARKS

We have analyzed self-diffusiophoresis of active colloids with solute being transported by diffusion from the colloid boundary, where it is produced (or consumed) axisymmetrically, to the bulk, where it is consumed (or produced) isotropically. The dimensionless problem is governed by the two associated surface and bulk Damköhler numbers, $\mathcal{S}$ and $\mathcal{B}$.

We have solved the problem using an eigenfunction expansion. This semianalytic solution, applicable for all values of $\mathcal{S}$ and $\mathcal{B}$, has been accompanied by asymptotic approximations. For small $\mathcal{S}$, the solute flux on the surface is effectively prescribed by the activity distribution $f(\theta)$; the resulting particle velocity is proportional to $\mathcal{S}$, with a coefficient that can be expressed explicitly as a function of $\mathcal{B}$ and f, see Eq. (5.5). For large $\mathcal{B}$, the solute concentration is uniform except within a boundary layer about the active portion of the boundary, and the particle velocity can be expressed explicitly as an integral of a function of $\mathcal{S}$, $\mathcal{B}$ and f, see Eq. (5.15). The linkage $\mathcal{S} \propto \mathcal{B}^{1/2}$ of a variable particle size constitutes a distinguished limit for that scenario. For $\mathcal{S} \gg \mathcal{B}^{1/2}$ (which includes the linkage $\mathcal{S} \propto \mathcal{B}$ of a variable solute diffusivity) we find that the particle velocity depends upon the relative fraction of the active boundary, but is otherwise indifferent to the activity details in that fraction. The associated boundary-layer solution breaks down near the edge of the active portion of the boundary. Following a similar analysis in a classical wave problem [14], we have obtained a closed-form solution of the local transport problem in the edge region.

We have neglected solute advection [15,16] in the present analysis. When accounting for advection, the conservation equation (3.5) generalizes to

$$\nabla^2 c - \mathrm{Pe}\, \mathbf{u} \cdot \nabla c = \mathcal{B} c, \tag{8.1}$$

wherein $\text{Pe} = a^* \mathcal{U}^* / D^*$ is the Péclet number. Generally speaking, then, the neglect of advection is justified if this number is small. Making use of Eq. (3.4) we see that

$$\text{Pe} = \frac{b^*(c_s^* - c_b^*)}{D^*}. \tag{8.2}$$

(Note that this intrinsic Péclet number, which is independent of particle size, differs from the standard one in the literature, which is based upon a typically over-simplified kinetic description.) It is interesting to note that the present large-$\mathcal{B}$ boundary-layer solution is likely valid even at large Pe as long as $\text{Pe} \ll \mathcal{B}$. The reason is that, with the boundary-layer thickness being $\mathcal{B}^{-1/2}$, the first (diffusive) term on the left-hand side of Eq. (8.1) is of order $\mathcal{B}$ while the second (advective) term on the left-hand side of Eq. (8.1) is of order Pe. [Note that the velocity (5.15) is $O(1)$.] The ratio of advection to diffusion is therefore of order $\text{Pe}/\mathcal{B}$.

To summarize, we recapitulate our results in terms of dimensional quantities. For weak interfacial activity, the particle velocity is proportional to $b^* k_-^* (c_s^* - c_b^*)/D^*$. In the limit of strong bulk activity, the solute concentration differs from c_b^* in a narrow boundary layer of thickness $(D^*/k_b^*)^{1/2}$. The resulting particle velocity scales as $b^*(c_s^* - c_b^*)/a^*$. Here, there are two situations. If the limit is realized by large values of a^*, the ratio of the particle velocity to $b^*(c_s^* - c_b^*)/a^*$ depends (nonlinearly) upon both the ratio $\alpha = k_-^*/(D^* k_b^*)^{1/2}$ and the activity profile. If the limit is realized by small values of D^*, the ratio of the particle velocity to $b^*(c_s^* - c_b^*)/a^*$ is independent of the reaction coefficients, the solute diffusivity, and even the details of the reaction profile.

APPENDIX: TRANSITION REGION

Following Lamb [17], we seek a solution of Eq. (6.4) of the form

$$C = e^{-Y} G + e^Y H. \tag{A1}$$

Requiring the functions G and H to satisfy

$$\frac{\partial^2 G}{\partial X^2} + \frac{\partial^2 G}{\partial Y^2} = 2\frac{\partial G}{\partial Y}, \quad \frac{\partial^2 H}{\partial X^2} + \frac{\partial^2 H}{\partial Y^2} = -2\frac{\partial H}{\partial Y}, \tag{A2}$$

Eq. (6.4) is trivially satisfied. To solve equations (A2), we employ the parabolic coordinates (see Fig. 1)

$$\xi = \rho^{1/2} \cos\frac{\vartheta}{2}, \quad \eta = \rho^{1/2} \sin\frac{\vartheta}{2}. \tag{A3}$$

These are natural for the transition-region geometry and conditions (6.7)–(6.8), since the negative real axis becomes $\xi = 0$, while the positive real axis becomes $\eta = 0$. With ξ and η as independent variables, Eq. (A2) become

$$\frac{\partial^2 G}{\partial \xi^2} + \frac{\partial^2 G}{\partial \eta^2} = 4\left(\eta\frac{\partial G}{\partial \xi} + \xi\frac{\partial G}{\partial \eta}\right), \quad \frac{\partial^2 H}{\partial \xi^2} + \frac{\partial^2 H}{\partial \eta^2} = -4\left(\eta\frac{\partial H}{\partial \xi} + \xi\frac{\partial H}{\partial \eta}\right). \tag{A4a, b}$$

The solution to Eq. (A4a) can be written as a combination of two similarity solutions

$$G = G_+(\zeta_+) + G_-(\zeta_-), \tag{A5}$$

wherein $\zeta_\pm = \xi \pm \eta$. We therefore obtain the ordinary differential equations

$$G_+'' = 2\zeta_+ G_+', \quad G_-'' = -2\zeta_- G_-', \tag{A6}$$

which integrate to give $G'_\pm = g_\pm e^{\pm \zeta_\pm^2}$. Similarly, the solution to Eq. (A4b) is written as a combination of two similarity solutions

$$H = H_+(\zeta_+) + H_-(\zeta_-). \tag{A7}$$

The resulting equations

$$H''_+ = -2\zeta_+ H'_+, \quad H''_- = 2\zeta_- H'_- \tag{A8}$$

integrate to give $H'_\pm = h_\pm e^{\mp \zeta_\pm^2}$.

Now, as $\rho \to \infty$, it is evident that $\zeta_+ \to \infty$ for all $0 < \vartheta < \pi$ while ζ_- tends to ∞ for $0 < \vartheta < \pi/2$ and to $-\infty$ for $\pi/2 < \vartheta < \pi$. To avoid a superexponential divergence of C at large ρ, which would clearly contradict Eq. (6.5), we must set $g_+ = h_- = 0$. We conclude that the most general solutions of Eq. (A4) are

$$G(\xi, \eta) = \grave{g} + g\,\mathrm{erf}(\xi - \eta), \quad H(\xi, \eta) = \grave{h} + h\,\mathrm{erf}(\xi + \eta). \tag{A9}$$

The four constants appearing in Eq. (A9) are determined from the boundary conditions. With condition (6.7) applying at $\xi = 0$ we readily obtain $\grave{h} = \grave{g}$ and $h = -g$. Thus, Eqs. (A1) and (A9) give

$$C = e^{-Y}[\grave{g} + g\,\mathrm{erf}(\xi - \eta)] + e^Y[\grave{g} - g\,\mathrm{erf}(\xi + \eta)]. \tag{A10}$$

Recalling that $\mathrm{erf}\,z \sim 1 - e^{-z^2}/z\sqrt{\pi}$ for $z \to \infty$, we must impose $\grave{g} = g$ to satisfy condition (6.5). Last, noting that the inhomogeneous condition (6.8) applies at $\eta = 0$, we readily obtain $g = 1/2$. We conclude that

$$C = \frac{e^{-Y}}{2}[1 + \mathrm{erf}(\xi - \eta)] + \frac{e^Y}{2}[1 - \mathrm{erf}(\xi + \eta)]. \tag{A11}$$

Substitution of Eq. (A3) yields Eq. (6.10).

---

[1] A. Aubret, S. Ramananarivo, and J. Palacci, Eppur si muove, and yet it moves: Patchy (phoretic) swimmers, Curr. Opin. Colloid Interface Sci. **30**, 81 (2017).

[2] R. Golestanian, T. B. Liverpool, and A. Ajdari, Designing phoretic micro-and nano-swimmers, New J. Phys. **9**, 126 (2007).

[3] J. L. Anderson, Colloid transport by interfacial forces, Annu. Rev. Fluid Mech. **21**, 61 (1989).

[4] S. Ebbens, M.-H. Tu, J. R. Howse, and R. Golestanian, Size dependence of the propulsion velocity for catalytic Janus-sphere swimmers, Phys. Rev. E **85**, 020401(R) (2012).

[5] P. de Buyl, A. S. Mikhailov, and R. Kapral, Self-propulsion through symmetry breaking, Europhys. Lett. **103**, 60009 (2013).

[6] O. Schnitzer, Weakly nonlinear dynamics of a chemically active particle near the threshold for spontaneous motion. I. Adjoint method, Phys. Rev. Fluids **8**, 034201 (2023).

[7] D. Sondak, C. Hawley, S. Heng, R. Vinsonhaler, E. Lauga, and J.-L. Thiffeault, Can phoretic particles swim in two dimensions? Phys. Rev. E **94**, 062606 (2016).

[8] E. Yariv, Two-dimensional phoretic swimmers: the singular weak-advection limits, J. Fluid Mech. **816**, R3 (2017).

[9] R. Brandão and E. Yariv, Spontaneous autophoretic motion of isotropic disks, J. Fluid Mech. **972**, R3 (2023).

[10] F. Picella and S. Michelin, Confined self-propulsion of an isotropic active colloid, J. Fluid Mech. **933**, A27 (2022).

[11] R. Brandão, Isotropically active particle closely fitting in a cylindrical channel: spontaneous motion at small Péclet numbers [J. Fluid Mech. (to be published)].

[12] N. Yoshinaga, K. H. Nagai, Y. Sumino, and H. Kitahata, Drift instability in the motion of a fluid droplet with a chemically reactive surface driven by Marangoni flow, Phys. Rev. E **86**, 016108 (2012).

[13] H. A. Stone and A. D. T. Samuel, Propulsion of microorganisms by surface distortions, Phys. Rev. Lett. **77**, 4102 (1996).

[14] A. Sommerfeld, Mathematische Theorie der Diffraktion: Mit einer Tafel, Math. Ann. **47**, 317 (1896).

[15] S. Michelin, E. Lauga, and D. Bartolo, Spontaneous autophoretic motion of isotropic particles, Phys. Fluids **25**, 061701 (2013).

[16] E. Yariv and S. Michelin, Phoretic self-propulsion at large Péclet numbers, J. Fluid Mech. **768**, R1 (2015).

[17] H. Lamb, On Sommerfeld's diffraction problem, and on reflection by a parabolic mirror, Proc. London Math. Soc. **s2-4**, 190 (1907).